

# Investigating AGN Heating in a Sample of Nearby Clusters

R.J.H. Dunn<sup>\*</sup> and A.C. Fabian

Institute of Astronomy, Madingley Road, Cambridge CB3 0HA

3 October 2018

## ABSTRACT

We analyse those objects in the Brightest 55 sample of clusters of galaxies which have a short central cooling time and a central temperature drop. Such clusters are likely to require some form of heating. Where clear radio bubbles are observed in these clusters, their energy injection is compared to the X-ray cooling rate. Of the 20 clusters requiring heating, at least 14 have clear bubbles, implying a duty cycle for the bubbling activity of at least 70 per cent. The average distance out to which the bubbles can offset the X-ray cooling,  $r_{\text{heat}}$ , is given by  $r_{\text{heat}}/r_{\text{cool}} = 0.86 \pm 0.11$  where  $r_{\text{cool}}$  is defined as the radius as which the radiative cooling time is 3 Gyr. 10 out of 16 clusters have  $r_{\text{heat}}/r_{\text{cool}} \gtrsim 1$ , but there is a large range in values. The clusters which require heating but show *no* clear bubbles were combined with those clusters which have a radio core to form a second sub-sample. Using  $r_{\text{heat}} = 0.86r_{\text{cool}}$  we calculate the size of an average bubble expected in these clusters. In five cases (3C129.1, A2063, A2204, A3112 and A3391) the radio morphology is bi-lobed and its extent similar to the expected bubble sizes. A comparison between the actual bubble size and the maximum expected if they were to offset the X-ray cooling exactly,  $R_{\text{max}}$ , shows a peak at  $R_{\text{bubble}} \sim 0.7R_{\text{max}}$  with a tail extending to larger  $R_{\text{bubble}}/R_{\text{max}}$ . The offset from the expected value of  $R_{\text{bubble}} \sim R_{\text{max}}$  may indicate the presence of a non-thermal component in the innermost ICM of most clusters, with a pressure comparable to the thermal pressure.

**Key words:** galaxies: clusters: general – galaxies: clusters: cooling flows – X-rays: galaxies: clusters

## 1 INTRODUCTION

Since the discovery of “holes” in the X-ray emission at the centre of the Perseus Cluster (Böhringer et al. 1993), and following the launch of *Chandra*, many more depressions in the intra-cluster medium (ICM) of low redshift clusters have been found (e.g. Hydra A, McNamara et al. 2000; A2052, Blanton et al. 2001; A2199, Johnstone et al. 2002; Centaurus, Sanders & Fabian 2002). Recent compilations are given in Dunn et al. (2005); Dunn & Fabian (2004); Bîrzan et al. (2004). Such holes have been observed to anti-correlate spectacularly with the radio emission from the active galactic nucleus (AGN) at the centres of these clusters. Their morphology, particularly in the closest clusters, has led to the interpretation that these are bubbles of relativistic gas blown by the AGN into the thermal ICM. This relativistic gas is less dense than the ICM and so the bubbles are expected to detach from the core and rise up buoyantly through the cluster, e.g. Perseus (Churazov et al. 2000; Fabian et al. 2003b). The older, detached, bubbles tend not to have GHz radio emission associated with them and have been termed “Ghost” bubbles.

The X-ray emission of the ICM naturally leads to the conclusion that the plasma should be cooling. To maintain pressure support, the gas is expected to flow on to the central galaxy

as a “cooling flow.” The subsequent increase in density would lead to a “cooling-catastrophe”, with extremely rapid cooling in the cluster centre. However, with the high spatial and spectral resolution of *Chandra* and *XMM-Newton* little of the expected X-ray emitting cool gas has been found (Peterson et al. 2003, see Peterson & Fabian 2006 for a review). Many mechanisms have been proposed by which the cool gas could be heated, including, for example, thermal conduction (Kim & Narayan 2003; Voigt & Fabian 2004), but this appears not to work for clusters below 5 keV.

A majority (71 per cent) of “cooling core” clusters harbour radio sources (Burns 1990), and a similar fraction of clusters which require heating (likely to be a cooling core) harbour clear bubbles (Dunn et al. 2005). The action of creating the bubbles at the centre of the cluster by the AGN is a favoured method of injecting energy into the central regions of the cluster and so prevent the ICM from cooling. This process sets up sound/pressure waves in the ICM, the dissipation of which requires the ICM to be viscous (Fabian et al. 2003b, 2006). The viscous dissipation of the pressure waves allows the energy from the bubble creation to be dissipated far from the cluster centre, as gentle, continuous and distributed heating as required (Voigt & Fabian 2004). Bîrzan et al. (2004) surveyed 80 clusters in the *Chandra* archive without discriminating between cooling and non-cooling clusters and found 16 that contained bubbles. This was interpreted as clusters having AGN/bubble

<sup>\*</sup> E-mail: rjhd2@ast.cam.ac.uk

**Table 1.** CLUSTER SAMPLE

Cluster	Redshift	ObsId	Exposure (ks)
2A 0335+096	0.0349	919	19.7
3C 129.1	0.0223	2219	9.6
A85	0.0521	904	38.4
A262	0.0164	2215	28.7
A478	0.0882	1669	42.4
A496	0.0223	931	18.9
A1644	0.0474	2206	18.7
A1651	0.086	4185	9.6
A1689	0.181	5004	19.9
A1795	0.0627	493	19.6
A2029	0.0767	891	19.8
A2052	0.0348	890	36.8
A2063	0.0355	6263	16.8
A2199	0.0300	497	19.5
A2204	0.1523	499	10.1
A2597	0.0824	922	39.4
A3112	0.0746	2516	16.9
A3391	0.0545	4943	18.4
A3558	0.0475	1646	14.4
A4059	0.0478	897	40.7
AWM7	0.0172	908	47.9
Centaurus	0.0109	4954	89.1
Cygnus A	0.0570	360	34.7
Hydra A	0.0522	4969	96.9
Klem44	0.0283	4992	33.5
M87	0.0037	2707	98.7
MKW3s	0.0449	900	57.3
Ophiuchus	0.028	3200	50.5
Perseus	0.0183	3209	95.8
PKS 0745-191	0.1028	508	28.0

All the clusters in the sample, for the sample selection see text. The exposure time is that after reprocessing the data.

activity only 20 per cent of the time. In this work we take a sample of clusters which forms a subset of an almost complete sample and investigate the bubble population therein. As the parent sample is almost complete we are able to investigate prevalence of cooling core clusters, duty cycles of bubble activity and radio sources within the general cluster population.

The sample selection is described in Section 2, and the data preparation and reduction in Section 3. The subset is itself then split into two: those clusters which are expected to require some form of heating and harbour clear bubbles; and a combination of those which require some form of heating but do not harbour bubbles and those clusters which have a central radio source. The analysis of those clusters with clear bubbles and of those without is discussed in Sections 4 and 5 respectively. The overall implications of this work is discussed in Section 6 with future investigations outlined in Section 7.

## 2 SAMPLE SELECTION

We use an updated version of the sample first outlined in Dunn et al. (2005), which is a subset of the Brightest 55 (B55) sample. The B55 sample was compiled by Edge et al. (1990) and studied in detail with *ROSAT* data from a cooling-time point of view by Peres et al. (1998). The B55 sample is a 2 – 10 keV flux-limited sample of clusters of galaxies which are close enough to have been

imaged by previous X-ray satellites, and is nearly flux complete at high galactic latitudes (all but nine are at  $b > |20^{\circ}|_{\text{circ}}$ ).

Out of the B55 sample, two clusters did not have *ROSAT* observations, and four only had *ROSAT HRI* observations. Out of the remaining 49 clusters, Dunn et al. (2005) selected those which had a short central cooling time ( $< 3$  Gyr) from the *ROSAT PSPC* and a large central temperature drop ( $T_{\text{outer}}/T_{\text{centre}} > 2$ ), as these would be the clusters requiring some form of heating so that large quantities of cool gas are not formed. Of the 49 clusters, 23 have a short  $t_{\text{cool}}$  and, using the most recent temperature profiles, 21 have a large central temperature drop. 20 clusters have both, of which 14 (70 per cent) show clear depressions (bubbles) in the X-ray emission from the Intra-Cluster Medium (ICM). The duty cycle of bubbling in clusters which require heating is therefore also at least 70 per cent. From the whole sample we find that the total fraction of clusters with clear bubbles from current observations is at least 25 per cent (14/55).

Of the six clusters which require heating but have no clear bubbles, only one has no radio source at the centre – AWM7 (Furusho et al. 2004). 2A 0335+096 has a complicated core structure, but there are depressions which have been interpreted as bubbles (Mazzotta et al. 2003) and so this cluster is included with those which have clear bubbles. MKW3s also has a faint depression further out from the centre, which has been interpreted as a bubble (Mazzotta et al. 2002) and this too is included with the clusters which have bubbles.

Also taken from the B55 sample are those clusters which are not already in the sample and which host a radio core at the centre, regardless of whether a *ROSAT* observation exists. The NVSS<sup>1</sup> was used to find central radio sources. The NVSS has extensive, but not complete sky coverage, and is not very deep, so clusters which harbour faint central sources will be missed<sup>2</sup>. Out of the clusters not already in the sample, at least another 10 which have a central radio source in the NVSS. So the fraction of clusters which have a central radio source is at least  $\sim 53$  per cent (29/55, i.e. including those with bubbles). These two cluster samples contain a total of 30 clusters (see Table 1), 16 of which have a radio source, clear bubbles and require heating<sup>3</sup>, 13 which have a radio source but no bubbles, and AWM7 which has no evidence for radio activity. The assignment of the clusters to the different groups is shown in Table 2.

We have chosen a central cooling time of  $t_{\text{cool}} < 3$  Gyr to investigate those clusters where a cooling flow would form if there is no heating. These are therefore the clusters in which extreme heating rates are expected. Changing to  $t_{\text{cool}} < 7$  Gyr  $\sim t_{\text{Hubble}}/2$  could add another nine clusters into the sample which require heating. There is only one cluster of these nine which also has a central temperature drop – A2142 – and so the fraction of clusters with bubbles from those which require heating changes little. Three of these nine clusters (A2063, A1689 & A1651) already fall into the sample which have core radio detections. None has a report of clear bubbles.

<sup>1</sup> NRAO (National Radio Astronomy Observatory) VLA (Very Large Array) Sky Survey

<sup>2</sup> For example, Marković et al. (2004) present new detections of central sources in A1650 and A2142 which are not detected in the NVSS.

<sup>3</sup> Donahue et al. (2005) investigate both A1650 and A2244 as they have radio-quiet cooling cores ( $t_{\text{cool}} < H_0^{-1}$ ). A2244 has  $t_{\text{cool}} > 3$  Gyr from Peres et al. (1998) and although Marković et al. (2004) detect a radio source at the centre of A1650 none is seen in the NVSS and so neither is in our sample.

**Table 2.** CLUSTER SUB-SAMPLES

Clear Bubbles		NVSS Radio		No Radio
Heating	Heating	No Heating	Heating	
A85	2A 0335+096 <sup>†</sup>	3C 129.1	AWM7	
A262	A496	A1644		
A478	A2204	A1651		
A1795	PKS 0745-191	A1689		
A2029	MKW3s <sup>†</sup>	A2063		
A2052		A3112		
A2199		A3391		
A2597		A3558		
A4059		Klem44		
Centaurus		Ophiuchus		
Cygnus A				
Hydra A				
M87				
Perseus				
14	5	10	1	

NOTES: <sup>†</sup> These clusters have complicated cores/faint depressions and are added to the Clear Bubbles set (for further discussion see text). The Clear Bubbles (incl <sup>†</sup>) clusters form one subset and the remainder form the other.

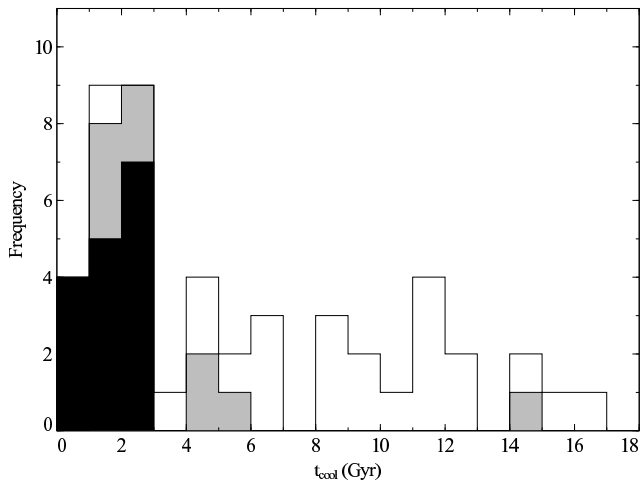


**Figure 1.** The distribution of  $t_{\text{cool}}$  in the B55 sample. The black bars indicate those clusters with clear bubbles, the grey are for the clusters with no bubbles but with radio sources. This graph has been truncated, two clusters with  $t_{\text{cool}} = 22$  and  $32$  Gyr (A1367 & A2255) have been removed to expand the  $x$ -axis.

## 2.1 Heating Distribution

The distribution of the central cooling times of the B55 clusters is shown in Fig. 1. Almost all of the clusters which have a cooling time less than 3 Gyr contain a radio source or clear bubbles, with the exception being AWM7. The clusters in the B55 sample which do not have central cooling time values from the *ROSAT PSPC* have not been included in the figure.

## 3 DATA PREPARATION

The X-ray *Chandra* data of the clusters were processed and cleaned using the CIAO software and calibration files (CIAO v3.3, CALDB v3.2). We began the reprocessing by removing the afterglow detec-

tion and re-identifying the hot pixels and cosmic ray afterglows, followed by the tool `ACIS_PROCESS_EVENTS` to remove the pixel randomisation and to flag potential background events for data observed in Very Faint (VF) mode. The Charge-Transfer Efficiency was corrected for, followed by standard grade selection. Point-sources were identified using the `WAVDETECT` wavelet-transform procedure. For clusters observed with the ACIS-S3 chip, the ACIS-S1 chip was used to form the light curves where possible. In all other cases, light-curves were taken from on-chip regions as free as possible from cluster emission. For the spectral analysis, backgrounds were taken from the CALDB blank-field data-sets. They had the same reprocessing applied, and were reprojected to the correct orientation.

Cluster centroids were chosen to lie on the peak in the X-ray surface brightness. Annular regions were automatically assigned with constant signal-to-noise, stopping where the calculated surface brightness of the cluster dropped below zero. The initial signal-to-noise was 100, and this was increased or decreased by successive factors of  $\sqrt{2}$  to obtain a number of regions between four and ten. The minimum signal-to-noise allowed was 10.

The 0.5 – 7 keV spectra were extracted, binned with a minimum of 20 counts per bin, and, using `XSPEC` (v12.2.1r) (e.g. Arnaud 1996), a `PROJECT` single temperature `MEKAL` (e.g. Mewe et al. 1995) model with a `PHABS` absorption was used to deproject the cluster. In some clusters the temperatures for some of the regions were undefined. To solve this problem, the minimum number of regions was reduced, a maximum radius for the outermost annulus was set, or the outermost region was removed to try to improve the behaviour of the profile (this was required for 3C129.1, A496, A1689, A2063, A2597, A3391, A4059, Klem 44, Ophiuchus & PKS0745). Using the deprojected cluster temperature, abundance and normalisation profiles; density, pressure, entropy, cooling time and heating profiles were created. The temperature profiles and the derived profiles for the clusters with clear bubbles are shown in the Appendix (Figs. 9 to 15).

These profiles give azimuthally averaged values for the cluster properties and have been used in the subsequent calculations. In some clusters, notably M87 and Perseus, the central parts of the cluster are not very smooth, e.g. due to bubbles. Donahue et al. (2006) show that these features do not strongly bias estimates of the entropy. As such the use of these azimuthally averaged values is not likely to introduce large biases into the subsequent calculations.

## 4 CLUSTERS WITH BUBBLES

To estimate the energy input of the AGN to the ICM we estimated the energy required to create the observed bubbles. If the expansion rates are slow then this is the sum of the bubble’s internal energy and the  $P_{\text{th}}dV$  work done.

$$E = \frac{1}{\gamma_1 - 1} P_{\text{th}} V + P_{\text{th}} V = \frac{\gamma_1}{\gamma_1 - 1} P_{\text{th}} V \quad (1)$$

where  $V$  is the volume of the bubble,  $P_{\text{th}}$  is the thermal pressure of the surrounding ICM and  $\gamma_1$  is the mean adiabatic index of the fluid in the bubble. In the case where the fluid in the bubble is relativistic,  $\gamma_1 = 4/3$ , and so the total energy in the bubble is  $4P_{\text{th}}V$ . As the bubbles are approximately elliptical we parameterise with a semi-major axis along the jet direction,  $R_1$ , and a semi-minor axis across it  $R_w$ . The volumes are therefore  $4\pi R_1 R_w^2/3$ , where we have assumed that the bubbles are prolate ellipsoids.

To obtain an estimate for the rate at which energy from a bubble would be dissipated in the ICM, the age for the bubble,  $t_{\text{age}}$ ,

is required. Most of the bubbles in the sample are young and still attached to their radio core. In these cases the timescale used is the sound speed timescale ( $t_{\text{age}} = t_{c_s} = R/c_s$ ) where the sound speed is given by

$$c_s = \sqrt{\gamma_2 k_B T / \mu m_H} \quad (2)$$

where  $\gamma_2 = 5/3$  for a non-relativistic gas. This timescale arises from the fact that no strong shocks have been observed in clusters. From this the bubbles are assumed to be expanding at not much more than the local sound speed of the ICM. In the cases where the bubbles are ghost bubbles, i.e. they do not contain GHz radio emission and are detached from the cluster centre, we have used the buoyancy timescale ( $t_{\text{age}} = t_b = R/v_b$ ) as these are expected to be rising buoyantly up through the ICM, with the buoyancy velocity given by

$$v_b = \sqrt{2gV/SC_D} \quad (3)$$

where  $C_D = 0.75$  is the drag coefficient (Churazov et al. 2001) and  $S = \pi r_w^2$  is the cross-sectional area of the bubble. Those bubbles which have been classed as Ghost bubbles are indicated in Table 3. For further discussion on the timescales see Section 6.2 and Dunn et al. (2005); Dunn & Fabian (2004). The energies and timescales for the bubbles were calculated from values for the radii in Allen et al. (2006); Dunn et al. (2005); Dunn & Fabian (2004), except for 2A 0335+096 which are from Birzan et al. (2004).

From the density profiles and the relevant cooling function, the heat input required per spherical shell was calculated. By comparing this to the total power provided by the bubble ( $P_{\text{bubble}} = 4P_{\text{th}}V/t_{\text{age}}$ ), the radius out to which the bubble power can offset the X-ray cooling was calculated for each cluster ( $r_{\text{heat}}$ , see Table 3). The radius is quoted in kpc and also as a fraction of  $r_{\text{cool}}$  (for a cooling time of 3 Gyr). For an estimate on the uncertainties, Monte-Carlo simulations of the calculations were performed.

The bubbles in A2052, Cygnus A and Perseus supply enough energy to offset all the X-ray cooling far beyond the cooling radius. In fact the energy they supply offsets all the X-ray cooling in the analysed regions of the cluster. In the Perseus cluster this is mainly because the cluster is so close, and so only the innermost regions fit onto one chip. In A2052 and Cygnus A the surface brightness of the X-ray emission falls to zero before the edge of the chip. As a result the spectral analysis stops at a radius such that the bubble energy offsets more than all the X-ray cooling within that radius. In the case of M87, the cluster is so close that the cooling radius,  $r_{\text{cool}}$ , could not be calculated from a single chip; however the bubble energy is greater than the X-ray cooling within the largest radius obtained on a single chip. These clusters are highlighted in Table 3. The results for M87 obtained from Ghizzardi et al. (2004) are shown for comparison and indicate that the current jet and counter jet cavities approximately offset all the X-ray cooling within  $r_{\text{cool}}$ . This result, however, has not been included in any of the subsequent analysis except where explicitly stated.

The average distance, as a fraction of the cooling radius, out to which the bubbles can offset the X-ray cooling is estimated using the mean of the results in Table 3. The uncertainties in the mean were estimated using a simple bootstrapping method. As a fraction of the cooling radius the mean distance out to which the bubbles offset the X-ray cooling is  $r_{\text{heat}}/r_{\text{cool}} = 0.86 \pm 0.11$ . The mean power that the bubbles supply, as a fraction of the X-ray cooling within the cooling radius, is  $0.89 \pm 0.16$ . The distribution of the distance out to which the bubbles offset the X-ray cooling is shown in Fig. 3. The clusters where the bubble power is such that it is greater than the all X-ray cooling within the analysed region

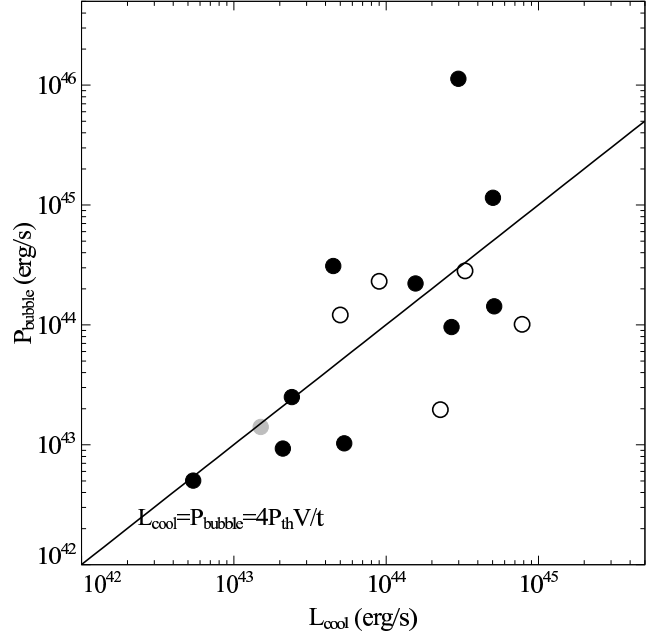


**Figure 2.** The X-ray Luminosity within the cooling radius versus the bubble power for the clusters. Clusters that fall above the line have AGN which inject sufficient energy into the ICM to offset all of the X-ray cooling. The four clusters with open circles are those with Ghost bubbles (2A 0335, A2597, A85, A478 and MKW 3s). The grey point is M87 using the data from Ghizzardi et al. (2004).

(A2052, Cygnus A & Perseus) and M87 have not been included in the estimate on the mean. Adding A2052, Cygnus A and Perseus into the estimation of the mean gives  $r_{\text{heat}}/r_{\text{cool}} = 1.45 \pm 0.29$  (with a heated fraction of  $3.49 \pm 1.93$ ), and so it is likely that the value of  $r_{\text{heat}}/r_{\text{cool}} = 0.86$  is a lower limit for this sample of clusters. See Section 6 for further discussion of the range of  $r_{\text{heat}}/r_{\text{cool}}$  and its implications. Comparing  $L_{\text{cool}}$  with  $P_{\text{bubble}}$  (Fig. 2) shows that there is a slight correlation between the cooling luminosity and the bubble power. The clusters lying above have AGN which supply sufficient energy into the ICM to offset the cooling.

In a set of clusters harbouring clear bubbles Birzan et al. (2004) and Rafferty et al. (2006) found that the mechanical luminosities required to offset the cooling ranged between  $1P_{\text{th}}V$  and  $20P_{\text{th}}V$ . Around half the objects in their sample had cavities which (assuming  $4P_{\text{th}}V$ ) could offset the cooling though there is a large spread, with some objects falling short. In this sample, which is drawn from an almost flux-complete parent sample, we find similar results.

As yet the method by which the bubbles dissipate their energy into the ICM has not been clearly determined. The energy also needs to be transported out to a large radius, for example, the viscous dissipation of sound waves in the ICM as they travel out in the cluster (Fabian et al. 2003a, 2005). As these are seen at large radii, they can plausibly carry their energy sufficiently far out. As a result, the bubbles analysed here, on average, supply enough energy to offset the X-ray cooling, but whether this energy actually performs this function is currently unknown.

**Table 3.** BUBBLE HEATING

Cluster	Bubble	Ghost?	$r_1$ (kpc)	$r_w$ (kpc)	$R_{\text{dist}}$ (kpc)	$L_{\text{cool}}^a$ $10^{43} \text{ erg s}^{-1}$	$r_{\text{cool}}$ (kpc)	$r_{\text{heat}}$ (kpc)	$r_{\text{heat}}/r_{\text{cool}}^b$	Heated Fraction <sup>c</sup>
2A 0335	E	G	9.3	6.3	23	$22.7 \pm 0.4$	$69.8 \pm 1.0$	$14.8 \pm 1.62$	$0.21 \pm 0.02$	$0.09 \pm 0.02$
	W	G	4.8	2.6	28					
A85	N	G	5.3	7.0	14	$9.0 \pm 0.4$	$47.6 \pm 1.3$	$81.4 \pm 10.7$	$1.71 \pm 0.23$	$2.54 \pm 0.71$
	S	G	6.4	8.6	22					
A262	E		2.4	1.8	3.2	$0.5 \pm 0.0$	$31.4 \pm 0.8$	$28.9 \pm 3.20$	$0.92 \pm 0.10$	$0.93 \pm 0.10$
	W		2.7	1.9	3.4					
A478	NE	G	4.0	6.9	9.8	$78.2 \pm 3.0$	$84.8 \pm 2.7$	$18.8 \pm 2.63$	$0.22 \pm 0.03$	$0.13 \pm 0.02$
	SW	G	4.5	7.7	10.7					
A1795	NW		4.1	3.1	3.8	$26.9 \pm 2.1$	$68.8 \pm 3.3$	$38.1 \pm 1.63$	$0.55 \pm 0.04$	$0.35 \pm 0.04$
	S		4.8	2.8	5.2					
A2029	NW		7.2	2.2	9.4	$51.2 \pm 9.4$	$73.3 \pm 9.9$	$31.9 \pm 3.50$	$0.43 \pm 0.08$	$0.31 \pm 0.08$
	SE		6.5	2.9	9.4					
<b>A2052</b>	N		10	10	10	$4.5 \pm 0.1$	$46.2 \pm 1.0$	$226 \pm 0.00$	$4.90 \pm 0.11$	$6.83 \pm 0.83$
	S		15	15	15					
A2199	E		2.3	1.3	2.3	$5.3 \pm 0.3$	$46.0 \pm 1.1$	$16.7 \pm 0.92$	$0.36 \pm 0.02$	$0.20 \pm 0.03$
	W		2.4	1.4	2.4					
A2597	NE	G	7.8	7.8	21	$33.0 \pm 1.5$	$66.6 \pm 1.0$	$63.2 \pm 5.08$	$0.95 \pm 0.08$	$0.85 \pm 0.14$
	SW	G	12	7.8	25					
A4059	N		5.4	2.2	5.4	$2.4 \pm 0.2$	$45.5 \pm 2.0$	$46.91 \pm 3.22$	$1.03 \pm 0.08$	$1.06 \pm 0.18$
	S		3.9	4.8	3.9					
Centaurus	E		2.8	1.7	2.5	$2.1 \pm 0.0$	$42.8 \pm 0.2$	$20.7 \pm 2.99$	$0.48 \pm 0.07$	$0.44 \pm 0.07$
	W		2.7	2.0	3.0					
<b>Cygnus A</b>	E		30	21	44	$29.8 \pm 1.1$	$55.1 \pm 1.6$	$359 \pm 0.00$	$6.52 \pm 0.19$	$38.0 \pm 5.8$
	W		34	22	48					
Hydra <sup>d</sup>	N		20	5.5	18	$15.6 \pm 0.2$	$56.2 \pm 0.7$	$83.5 \pm 11.6$	$1.49 \pm 0.21$	$1.42 \pm 0.14$
	S		17	4.4	22					
<b>M87</b>	E		1.5	1.5	1.5	$2.5 \pm 0.0$	$27.4 \pm 0.0$	$27.4 \pm 0.00$	$1.00 \pm 0.00$	$0.66 \pm 0.02$
	W		1.9	1.2	1.9					
MKW3s	S	G	13	21	56	$5.0 \pm 0.3$	$53.4 \pm 2.0$	$110 \pm 29.7$	$2.06 \pm 0.56$	$2.48 \pm 0.67$
	N		8.2	8.2	8.2	$50.2 \pm 0.1$	$76.4 \pm 0.1$	$109 \pm 0.00$	$1.43 \pm 0.00$	$2.29 \pm 0.03$
<b>Perseus</b>	S		8.9	8.9	8.9					
M87 <sup>e</sup>	E		1.5	1.5	1.5	$1.5 \pm 0.1$	$37.4 \pm 2.3$	$35.3 \pm 3.0$	$0.94 \pm 0.10$	$0.93 \pm 0.15$
	W		1.9	1.2	1.9					

The clusters in bold are those where the bubbles heat beyond the analysed region. For M87 the cooling radius could not be determined from a *ACIS* single chip. These clusters were not included in the calculation of the mean values.

<sup>a</sup>  $L_{\text{cool}}$  calculated for the 0.5 – 7.0 keV range. <sup>b</sup> The radius, as a fraction of the cooling radius, out to which the bubble power ( $4P_{\text{th}}V/t_{\text{age}}$ ) can offset the X-ray radio source by interacting with its surroundings cooling. <sup>c</sup> The fraction of the X-ray cooling that occurs within the cooling radius which is offset by the energy of the bubble's expansion. <sup>d</sup> The bubble sizes for Hydra A are not those from the cluster scale outburst from Nulsen et al. (2005) but from the smaller, inner radio emission. <sup>e</sup> These values for M87 come from the data in Ghizzardi et al. (2004) which extend to larger radii.

## 5 CLUSTERS WITHOUT BUBBLES

The second cluster subset is a combination of those clusters which require heating and show *no* clear bubbles, and those clusters which harbour a radio source (see Table 2). The amount of X-ray cooling within  $r_{\text{heat}}/r_{\text{cool}} = 0.86$  (the mean distance out to which the bubbles offset the X-ray cooling for the other cluster subset) for these clusters was calculated. In the assumption that any X-ray cooling from these clusters is also offset by AGN bubbles, and that these bubbles are young and so expanding at the sound speed, the dimensions of these bubbles was calculated. The resulting dimensions are shown in Table 4, where we have assumed that bubbles occur in pairs. The uncertainties have been estimated using simple Monte-Carlo simulations of the calculation.

The total X-ray counts expected within the area of the predicted bubble in the current observation was calculated from the average X-ray counts per pixel in the central regions of the cluster. The central regions were chosen so that it could be reasonable assumed that the surface brightness is constant. This is, however,

a lower limit on the number of counts and the signal to noise for the innermost regions, i.e. those where any bubbles are likely to be. This gave the expected X-ray signal to noise which is shown in Table 4. Using the bubbles in A2052 and Hydra A as templates, we estimate that the counts in the centre of the bubbles are around 30 percent lower than the counts in the rims.

So that any bubbles could be detected above the noise at a  $3\sigma$  level the X-ray signal to noise has to be greater than around 10 (equivalent to noise at 10 per cent level). This does, however, rely on knowing where the bubbles are in the centre of the cluster. If there is extended radio emission then the average counts interior and exterior to the expected bubble can be compared to see if there is a net decrement within the bubble. Half of the clusters in the sample have signal-to-noise values of less than 10, and so, even if extended radio emission is detected, no significant detection of bubbles from the current X-ray observations are likely. The counts per pixel in the central regions of these clusters is also very low.

A496, A2204, A3112, AWM7, Klem44, Ophiuchus and PKS 0745 all have X-ray signal-to-noise which is such that if a

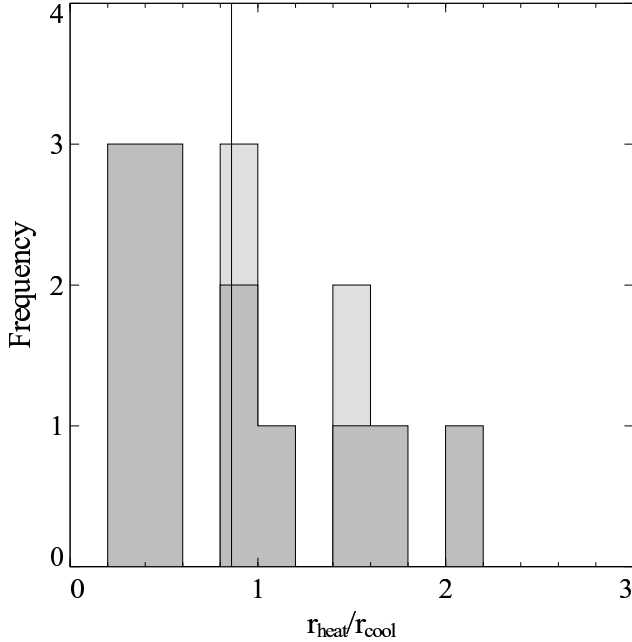


**Figure 3.** The distribution of the radius (as a fraction of the cooling radius) out to which the energy in the bubbles can offset the X-ray cooling. The extra points at  $r_{\text{heat}}/r_{\text{cool}} = 0.8 - 1$  and  $r_{\text{heat}}/r_{\text{cool}} = 1.4 - 1.6$  are M87 and Perseus respectively. A2052 and Cygnus A are not included on this plot. All four of these clusters were not taken into account when calculating the mean, indicated by the vertical line.

bubble of the expected size were present it should be detectable in the current X-ray observation. This is, however, still with the caveat that the size and location of the bubble is known (again, extended radio emission would help with this).

To be able to detect a decrement in the X-ray emission without any radio emission to guide the eye is more difficult. AWM7 and Klem44 only have around one count per pixel in the central regions, and so it is unlikely that a bubble could be identified by eye from the X-rays alone. It is more likely that in clusters with higher counts per pixel (A2204, Ophiuchus and PKS 0745) that bubbles would be detectable as these have more than 1000 counts expected within the area of the expected bubble.

The contrast ratio we have chosen, however, is for very clear bubbles with well defined rims in nearby clusters. In smaller radio sources, bubbles may be less clearly defined, and so the X-ray signal-to-noise may have to be much higher to be able to clearly detect cavities if they are there.

Using the Very Large Array (VLA)<sup>4</sup> and Australia Telescope Compact Array (ATCA)<sup>5</sup> archives we attempted to find observations of these clusters to investigate the morphology of the radio sources at their centres. In most cases the radio sources were not resolved in the archival observations. However for at least four of the clusters in Table 4 there are extended radio sources which could be bubbles that have not been detected in the X-ray images of clusters. In other cases it has not been possible to find radio data of high

<sup>4</sup> The National Radio Astronomy Observatory is operated by Associated Universities, Inc., under cooperative agreement with the National Science Foundation.

<sup>5</sup> The Compact Array is part of the Australia Telescope, which is funded by the Commonwealth of Australia for operation as a National Facility managed by CSIRO.

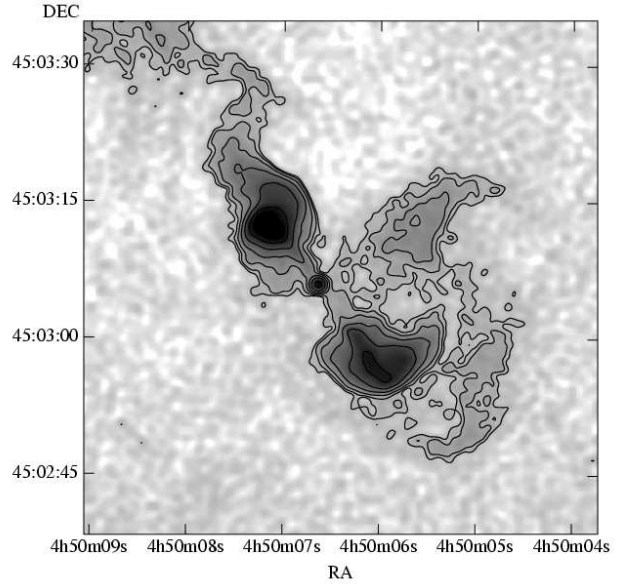


**Figure 4.** The 5 GHz radio emission from 3C129.1 (Taylor et al. 2001).

enough resolution, and so there may be further clusters with, as yet, undetected bubbles.

In the case of 3C 129.1 the morphology of the radio emission is very suggestive that the surrounding ICM is constraining the expansion of the inner radio lobes (see Fig. 4). The X-ray observations to date, however, show no clear interactions of the radio source with the ICM. The observed radio lobes in 3C 129.1 are  $\sim 2.6$  kpc (5.5 arcsec) in radius, which is around four times that expected for an “average” bubble in this cluster,  $0.60 \pm 0.16$  kpc ( $1.34 \pm 0.36$  arcsec). The observed radio lobes correspond to around 10 *Chandra* pixels in radius (which are  $0.49 \times 0.49$  arcsec), and so if the radio lobes are excavating cavities in the ICM, then the resultant bubbles should be seen in deep X-ray observations of the cluster which would increase the X-ray signal-to-noise.

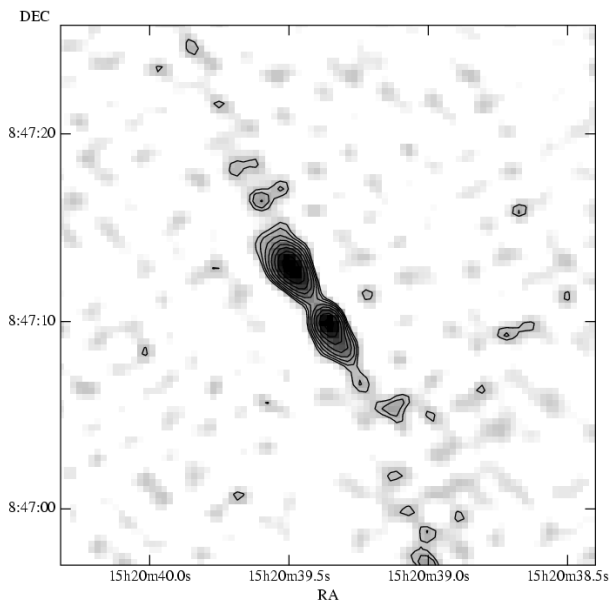
A3391 also harbours an extended radio source with a bilobed morphology (Otani et al. 1998; Morganti et al. 1999). The radio lobes in this cluster are separate from the radio core. If these lobes have formed cavities in the ICM, this separation implies that the cavities are older bubbles which have detached from the cluster centre and are rising buoyantly. The radio structure is not smooth and simple, but the 13 cm (2.38 GHz) observations from Otani et al. (1998) show the lobes as  $\sim 8 \times 12$  kpc ( $8 \times 12$  arcsec or  $16 \times 24$  *Chandra* pixels) in size. The expected size of an average bubble is  $2.61 \pm 0.33$  kpc, which is much smaller than the observed size of the radio emission.

The *ROSAT* X-ray maps of the centre of this cluster show no clear indication that the radio source is interacting with its surroundings. An explanation for these large detached radio lobes is if close feedback exists between the X-ray cooling and the AGN heating, then there may recently have been a past cycle of AGN heating and now there is a period of quiescence and no (small) lobes are seen with the expected sizes.

The central radio source in A2063 also has two peaks of emission. The dimensions of the observed radio emission are  $\sim 2 \times 1$  arcsec corresponding to  $\sim 1.4 \times 0.7$  kpc (or  $4 \times 2$  *Chandra* pixels). The expected sizes for average radio bubbles in this cluster are  $2.09 \pm 0.38$  kpc ( $2.95 \pm 0.53$  arcsec or  $\sim 6$  *Chandra* pixels) in size.

**Table 4.** PREDICTED BUBBLE SIZES

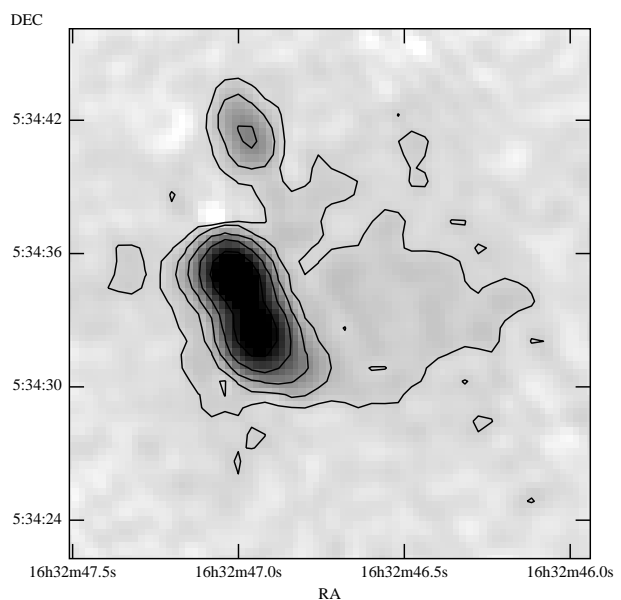
Cluster	$r_{\text{cool}}$ (kpc)	Predicted Bubble Radius (kpc)		X-ray S/N	counts/pix
			arcsec		
3 C129.1	$5.89 \pm 3.08$	$0.60 \pm 0.16$	$1.34 \pm 0.36$	0.9	0.04
A496	$54.83 \pm 1.97$	$5.50 \pm 0.53$	$8.40 \pm 0.80$	53.7	3.15
A1644	$24.55 \pm 9.05$	$1.98 \pm 0.34$	$2.13 \pm 0.36$	4.6	0.37
A1651	$14.24 \pm 12.53$	$1.40 \pm 0.49$	$0.87 \pm 0.30$	1.5	0.22
A1689	$63.12 \pm 5.85$	$5.19 \pm 0.42$	$1.70 \pm 0.14$	7.0	1.32
A2063	$29.27 \pm 1.57$	$2.09 \pm 0.38$	$2.95 \pm 0.53$	6.5	0.37
A2204	$69.44 \pm 3.16$	$8.13 \pm 1.04$	$3.06 \pm 0.39$	34.1	9.56
A3112	$57.86 \pm 2.71$	$5.44 \pm 0.62$	$4.05 \pm 0.46$	30.4	4.34
A3391	$10.84 \pm 2.18$	$2.61 \pm 0.33$	$2.52 \pm 0.32$	2.5	0.08
A3558	$14.90 \pm 1.46$	$1.60 \pm 0.10$	$1.72 \pm 0.10$	4.0	0.41
AWM7	$24.84 \pm 2.34$	$1.25 \pm 0.22$	$3.58 \pm 0.63$	15.6	1.46
Klem44	$38.79 \pm 1.41$	$2.56 \pm 0.21$	$4.61 \pm 0.39$	16.1	0.94
Ophi	$32.85 \pm 0.82$	$1.69 \pm 0.32$	$3.01 \pm 0.57$	28.6	6.93
PKS 0745	$90.76 \pm 2.16$	$10.08 \pm 2.03$	$5.32 \pm 1.07$	51.9	7.31


**Figure 5.** The 4.9 GHz radio emission from A2063.

None of the X-ray observations of these three clusters are deep enough so that clear indications of an interaction between the radio source and the ICM are expected.

The 1.32 GHz radio map of A3112 shows two faint diffuse regions of emission to the south east and south west of the core (Takizawa et al. 2003). Unfortunately the radio image has an elongated beam which makes it difficult to determine whether a faint excess in the X-rays is definitely associated with the radio lobes. The observed radio emission is  $\sim 4$  arcsec in radius corresponding to  $\sim 5$  kpc (or  $\sim 8$  *Chandra* pixels). The emission is offset from the core, so it may correspond to detached bubbles which still have some GHz radio emission. The expected sizes for average radio bubbles in this cluster match almost exactly the observed radio emission.

A2204 and PKS 0745 are the two of the more distant clusters in our sample, with redshifts greater than 0.1 (0.1523 and 0.1028 respectively). The radio morphology of A2204 shows two clear maxima (see Fig. 6), which could be the two lobes of the ra-


**Figure 6.** The 1.5 GHz radio emission from A2204 (Sanders et al. 2005).

dio source, which have not been fully resolved. Again, the X-ray emission shows no clear indication of any interaction of the radio source with the ICM. The radii of the observed radio maxima in A2204 are  $\sim 5$  kpc ( $\sim 2$  arcsec or 4 *Chandra* pixels), and the size of the average bubble expected in this cluster is only slightly larger ( $8.13 \pm 1.04$  kpc or  $3.06 \pm 0.39$  arcsec).

PKS 0745 has an amorphous radio source at the cluster centre, rather than a clear bi-lobed morphology and it is unclear as to the effect of the central radio source on the ICM. The *total* dimensions of the observed radio source are  $9.2 \times 6.0$  kpc, which is not that dissimilar from that for an expected bubble ( $r = 10.1 \pm 2.0$  kpc).

The X-ray observations of these three clusters are sufficiently deep that if any bubbles existed and the surface brightness contrast between the rims and the bubble centre were only 10 per cent they should be observed, especially as there is extended radio emission to guide the eye. It is possible that the contrast between the bubbles and the surrounding rims in these two clusters is very low, and as a result any cavities have not yet been detected. In any case, deeper

X-ray observations would allow further investigation into the presence or absence of bubbles in these clusters.

The current X-ray observations for most of these clusters are too short to provide sufficient signal-to-noise for any cavities to be clearly identified in the images. As a result some cluster may harbour bubbles which cannot be detected. Some of the clusters do, however, harbour extended radio sources whose dimensions are not dissimilar to those expected from an “average” bubble, should one be present in the cluster.

## 6 DISCUSSION

We first discuss the spread in values of  $r/r_{\text{cool}}$  and then investigate the possibility of the young bubbles being below their maximum size. Finally we detail some of the uncertainties and biases present in this analysis.

Although the mean of the radius out to which the bubbles can offset the X-ray cooling is  $0.86r_{\text{cool}}$  (from bootstrapping), there is a large spread in the values (see Fig. 3). In some clusters the bubble power offsets the heating out to over  $1.5r_{\text{cool}}$  (Hydra) whereas in others it only reaches out to  $0.36r_{\text{cool}}$  (A2199). The range of the energy supplied by the bubbles as a fraction of that required within  $r_{\text{cool}}$  also has a large spread, from  $\times 1.4$  that required in Hydra, to  $\times 0.20$  in A2199, with an average of 0.89. The Ghost bubbles are not taken into account here, along with the clusters where the analysis is not complete (A2052, Cygnus A and Perseus, but not M87). Adding these in the range increases from 0.22 to  $6.5r_{\text{cool}}$ . So in some clusters the bubbles can provide (more than) enough heating to offset the X-ray cooling, but some fall short.

Fig. 7 shows the distance to which the bubbles can offset the X-ray cooling versus the central cooling time (from Peres et al. 1998 adjusted to our cosmology). The grey point is M87 using the data presented in Ghizzardi et al. (2004). The three squares are A2052, Cygnus A and Perseus where the bubbles provide energy to beyond where it was possible to deproject the cluster. Unfortunately there is no clear correlation between  $r/r_{\text{cool}}$  and  $t_{\text{cool}}$ .

Seven clusters have  $r/r_{\text{cool}} > 1$ , three have  $r/r_{\text{cool}} \sim 1$  and six have  $r/r_{\text{cool}} < 1$ . So in most (10 out of 16) of the clusters the energy supplied by the bubbles is sufficient to offset the X-ray cooling. Of the six which have insufficient, four have young, active bubbles. A possible explanation is that these bubbles are still growing and so have not reached their maximum size. Therefore they currently do not contain sufficient energy to offset the cooling, but may do at later stages in their evolution. For further discussion see Section 6.1.

The ghost bubbles are more difficult to explain as these bubbles would be expected to be at their final size. They are also those which supply the least amount of energy into the ICM. The cooling times at the centres of these clusters are very short ( $< 1$  Gyr) and so a comparatively large amount of heating is required to offset the X-ray cooling. It is possible that we have caught the AGN in a period of relative quiescence where the ICM is cooling and only small bubbles are produced. Once a reservoir of fuel for the AGN has built up from the ICM then if it goes into a major outburst the bubbles may be such that they offset the cooling.

### 6.1 Bubble Sizes

So far we have assumed that the bubbles in the clusters are at their “maximum” size, however is this true? Calculating the bubble radius expected if its energy were offsetting all the X-ray cooling we

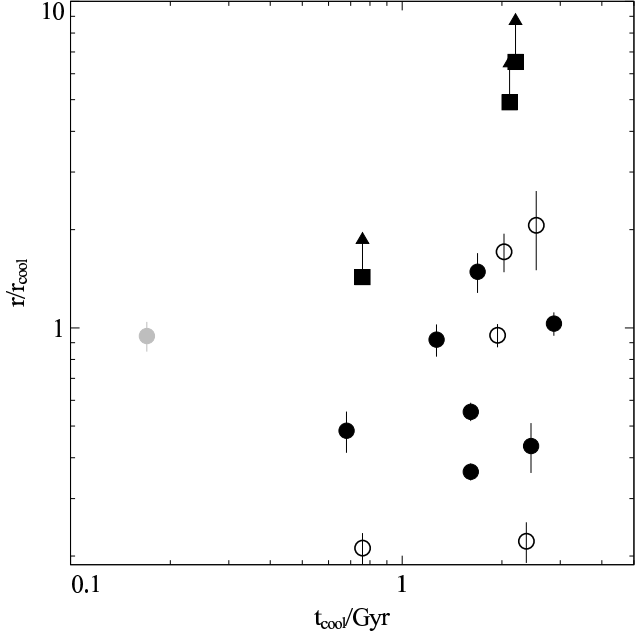


**Figure 7.** The distance out to which the bubbles can offset the X-ray cooling versus the central cooling time. The three clusters which have lower limits are Perseus, A2052 and Cygnus A (in increasing  $t_{\text{cool}}$ ). The four clusters with open circles are those with Ghost bubbles (2A 0335, A2597, A85, A478 and MKW 3s). The grey point is M87.

show that it is likely that our sample contains a large fraction of small bubbles.

If the jet supplying the bubbles is constant, then there is expected to be a continuous cycle of bubble growth with periodic detachment. As the radius of the bubble depends on the cube-root of the bubble age, most bubbles would be observed when they are close to their maximum sizes. From Churazov et al. (2000), in the assumption that the jet is of constant power and the bubbles are expanding subsonically,

$$\begin{aligned} \frac{\gamma_1}{\gamma_1 - 1} P_{\text{th}} V &= CLt \\ P_{\text{th}} \frac{4}{3} \pi R_{\text{max}}^3 &= \frac{\gamma_1 - 1}{\gamma_1} CLt_{\text{max}} \\ R_{\text{max}} &= \sqrt{\frac{3CL}{16\pi P_{\text{th}} v_{\text{grav}}}}. \end{aligned} \quad (4)$$

We naively assume that the numerical constant,  $C = 1$ ,  $\gamma_1 = 4/3$  and  $t_{\text{max}} = R_{\text{max}}/v_{\text{grav}}$ . Using the sound speed,  $v_{\text{cs}}$ , for  $v_{\text{grav}}$  as this depends only on the surrounding ICM and not the bubble size, and half the power required to balance cooling for  $L = L_{\text{cool}}/2$  (as there are two bubbles per cluster),  $R_{\text{max}}$  is calculated. This is the maximum size of the bubble possible if all the energy of its creation is converted to  $P_{\text{th}} V$  work on the ICM. The distribution of  $R_{\text{av}}/R_{\text{max}}$  is shown in Fig. 8, where  $R_{\text{av}} = \sqrt[3]{R_1 R_w^2}$ , the average radius of the observed bubble. Monte Carlo simulations of the data have been used to take into account the errors in the distribution and provide an estimate on the values of the bins<sup>6</sup>. All clusters

<sup>6</sup> The uncertainties on  $R_{\text{av}}/R_{\text{max}}$  result from the uncertainties in the input data, e.g. temperature profiles of the cluster. To obtain an estimate on the uncertainties on the values of the binned  $R_{\text{av}}/R_{\text{max}}$  distribution, the

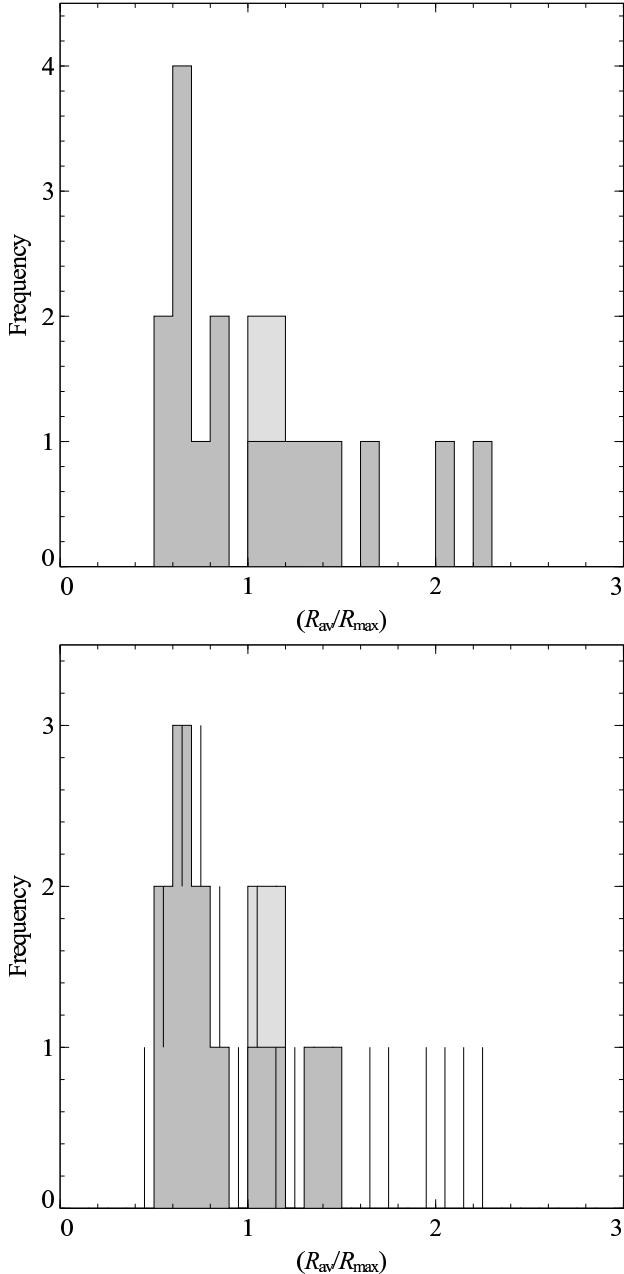


**Figure 8.** TOP: The distribution of bubbles as a fraction of their maximum size ( $R/R_{\max}$ ) assuming subsonic expansion. BOTTOM: The result of Monte Carlo simulations of the distribution in order to obtain errors (the vertical lines) on the distribution, and so a clearer indication of the true distribution. The lighter grey bars are from M87. The bubbles from Cygnus A and one from A2052 would appear off to the right of this plot.

with young bubbles (11 clusters, 22 bubbles) are included in the analysis and Fig. 8. As our analysis of M87 did not go far enough out in radius to obtain  $r_{\text{cool}}$  we used the temperature, and electron density profiles in Ghizzardi et al. (2004) to calculate  $R_{\text{av}}/R_{\text{max}}$ . The values of  $t_{\text{max}}$  and  $R_{\text{av}}/R_{\text{max}}$  are shown in Table 5.

The distribution peaks around  $\sim 0.7R_{\text{av}}/R_{\text{max}}$  with a tail

results were binned many times ( $10^4$  runs), assuming a Gaussian distribution of uncertainties in  $R_{\text{av}}/R_{\text{max}}$ . The inter-quartile range in the values for each of the bins is what is shown by the error bars.

extending to larger  $R_{\text{av}}/R_{\text{max}}$ . This implies that a large number of the bubbles have not yet attained their maximum size, and others are much larger than they “should” be.

The bubbles with a small  $R_{\text{av}}/R_{\text{max}}$  are likely to be young bubbles caught in the act of growing. They are not particularly younger than any other bubbles, but may be young for the cluster. For example, the inner bubbles in A2199, which have been analysed here, are very much smaller than the large scale radio emission, which also corresponds to clear decrements in the X-ray emission from the ICM. The large X-ray holes have  $R_{\text{av}} \sim 15$  kpc giving an  $R_{\text{av}}/R_{\text{max}} \sim 5$ , whereas the inner bubbles have  $R_{\text{av}} \sim 1.6$  kpc giving an  $R_{\text{av}}/R_{\text{max}} \sim 0.5$ . These bubbles are also those which do not supply sufficient energy to the ICM, which is unsurprising as we have used  $L_{\text{cool}}$  when calculating  $R_{\text{max}}$ .

As the bubbles with  $R_{\text{av}}/R_{\text{max}} \lesssim 1$  are likely to be young bubbles, it is possible that those bubbles with  $R_{\text{av}}/R_{\text{max}} \gtrsim 1$  may be those which have detached and are expanding as they rise up through the ICM.

Also, some of the clusters with  $R_{\text{av}}/R_{\text{max}} > 1$  have morphologies which are different to the younger ones. Hydra A may not have “bubbles” in the same way as the other clusters. The cluster-scale outburst reported in Nulsen et al. (2005) shows that the radio source has ploughed through the ICM rather than being confined by it; Cygnus A and A4059 are similar – there are X-ray decrements, but the synchrotron plasma is not totally confined by the ICM. It may be the case that the bubbles in A2052 and Perseus are just in the process of detaching, they still appear as young bubbles as the radio emission has not had time to decay, but they are at the maximum possible size for the cluster and are beginning to buoyantly rise. The bubble dimensions we have used for the Perseus cluster in this analysis are not those labelled as “Inner Bubbles” in Dunn et al. (2006). Using the radii for the Inner bubbles in this analysis ( $\sim 4$  kpc) gives an  $R_{\text{av}}/R_{\text{max}} \sim 0.6$ .

If we assume that most bubbles that we observe are at their maximum size, then we have overestimated  $R_{\text{max}}$ . To move the peak in the distribution, such that  $R_{\text{av}}/R_{\text{max}} \sim 1$ ,  $R_{\text{max}}$  has to reduce by a factor  $\sim 0.7$ . Which of the assumptions that we have used in the analysis could be changed to reduce  $R_{\text{max}}$ ?

We have assumed that the timescale over which the bubbles heat the ICM is the same as the sound speed timescale of the bubbles’ formation. Bubbles may grow in fits and starts (Fabian et al. 2005), the actual time taken to expand the bubble may be shorter, as there are periods where there is no expansion. Depending on the exact nature of the growth the true expansion time may be less than the one calculated. The energy dissipation time is also going to be different to the bubble creation timescale (see Section 6.2 for more discussion on this topic).

We have assumed  $\gamma_1 = 4/3$ , but if it is possible for  $\gamma_1 \sim 1.1$  then the peak of the distribution occurs at  $R_{\text{av}}/R_{\text{max}} \sim 1$ . A smaller value of  $\gamma_1$  means that the same amount of energy creates a smaller bubble than if  $\gamma_1 = 4/3$ . Investigations into the weak shock around the northern Perseus bubbles have shown it to be isothermal (Fabian et al. 2006), which requires an effective  $\gamma_2 \sim 1$  for the ICM. Further investigations are required to determine the true nature of  $\gamma$  in the radio bubbles and the ICM.

Sanders et al. (2005) find non-thermal X-rays from the central regions of the Perseus Cluster. These most likely arise from magnetic fields and cosmic rays in the ICM. Using the more recent 900 ks observation Sanders *et al.* (in prep) find that the non-thermal electron pressure within a radius of 40 kpc is comparable to the total thermal pressure. As a result the total pressure against which the bubbles are expanding is about twice that which has previously

**Table 5.**  $r_{\text{av}}/R_{\text{max}}$ 

Cluster	$R_{\text{av}}$ kpc	$P$ eV cm <sup>-3</sup>	$c_s$ 10 <sup>7</sup> cm s <sup>-1</sup>	$t_{\text{max}}$ 10 <sup>7</sup> yr	$R_{\text{av}}/R_{\text{max}}$
A262	1.97 ± 0.11	60.1 ± 0.7	4.90 ± 0.02	0.38 ± 0.01	1.04 ± 0.06
A1795*	2.11 ± 0.12	60.1 ± 0.7	4.90 ± 0.02	0.38 ± 0.01	1.11 ± 0.07
	3.40 ± 0.11	224 ± 11	9.62 ± 0.21	0.51 ± 0.03	0.68 ± 0.04
	3.35 ± 0.11	224 ± 11	9.62 ± 0.21	0.51 ± 0.03	0.67 ± 0.04
A2029*	3.23 ± 0.34	389 ± 16	10.9 ± 0.2	0.42 ± 0.04	0.70 ± 0.09
	3.79 ± 0.30	389 ± 16	10.9 ± 0.2	0.42 ± 0.04	0.81 ± 0.10
A2052	9.98 ± 0.51	70.2 ± 1.3	6.45 ± 0.04	0.67 ± 0.01	2.25 ± 0.12
	15.0 ± 0.8	70.3 ± 1.4	6.45 ± 0.04	0.67 ± 0.01	3.38 ± 0.18
A2199*	1.57 ± 0.06	148 ± 5	7.46 ± 0.10	0.40 ± 0.02	0.52 ± 0.04
	1.68 ± 0.06	148 ± 5	7.46 ± 0.10	0.40 ± 0.02	0.55 ± 0.04
A4059	2.98 ± 0.14	55.3 ± 2.4	6.57 ± 0.07	0.54 ± 0.03	0.82 ± 0.06
	4.47 ± 0.24	55.3 ± 2.4	6.57 ± 0.07	0.54 ± 0.03	1.23 ± 0.10
Centaurus*	1.97 ± 0.17	108 ± 1	4.75 ± 0.01	0.58 ± 0.01	0.70 ± 0.06
	2.25 ± 0.16	108 ± 1	4.75 ± 0.01	0.58 ± 0.01	0.79 ± 0.06
Cygnus A	23.7 ± 1.2	448 ± 44	13.4 ± 0.5	0.23 ± 0.02	7.64 ± 0.55
	25.1 ± 1.2	454 ± 40	13.4 ± 0.5	0.23 ± 0.02	8.12 ± 0.57
Hydra	8.44 ± 0.40	204 ± 6	8.53 ± 0.12	0.48 ± 0.01	2.01 ± 0.10
	6.85 ± 0.38	208 ± 23	8.55 ± 0.12	0.47 ± 0.03	1.69 ± 0.07
Perseus	8.15 ± 0.00	306 ± 2	8.98 ± 0.05	0.65 ± 0.01	1.36 ± 0.01
	8.89 ± 0.00	306 ± 2	8.98 ± 0.05	0.65 ± 0.01	1.49 ± 0.01
M87	1.35 ± 0.03	272 ± 22	6.54 ± 0.20	0.19 ± 0.02	1.04 ± 0.07
	1.51 ± 0.03	272 ± 22	6.54 ± 0.20	0.19 ± 0.02	1.16 ± 0.08

The average bubble radius ( $R_{\text{av}}$ ), ICM pressure, sound speed ( $V_s$ ) and  $R_{\text{av}}/R_{\text{max}}$  for all the young bubbles in the sample. The starred clusters are those in which the bubbles do not provide sufficient energy to offset the X-ray cooling.

been estimated. Amending Equation 4 results in

$$R'_{\text{max}} = \sqrt{\frac{3CL}{16\pi(2P_{\text{th}})v_{\text{grav}}}} = \frac{R_{\text{max}}}{\sqrt{2}} = 0.7R_{\text{max}}. \quad (5)$$

If the non-thermal components are taken into account, then  $R_{\text{max}}$  reduces by the factor of 0.7 required. As the distribution of  $R_{\text{av}}/R_{\text{max}}$  peaks at around 0.7 then it is likely that a non-thermal component of the ICM exists and is important in the innermost regions of all cool core clusters. We note that the possible presence of a non-thermal pressure component was suggested by Voigt & Fabian (2006) from determination of mass profiles in cool core clusters.

## 6.2 Timescales

The timescales used to calculate the power output into the cluster by the creation of bubbles have been those of the sound speed. So far no strong shocks have been observed around the rims of the bubbles. This means that they are currently expanding at less than the sound speed. We therefore have an upper limit on the bubble expansion time, which has been used as the timescale over which the bubbles deposit energy into the ICM.

This is the bubble expansion timescale, however, rather than the timescale over which the bubbles dissipate their energy in the ICM. We have so far assumed that these two timescales are equivalent. But, as the bubbles can still be seen in the form of detached ghost bubbles (e.g. Perseus & Centaurus), bubbles last longer than this timescale. As such the energy is dissipated over a longer timescale than has been assumed here.

If bubbles are continually produced, so the moment one detaches, or shortly thereafter, another one starts to form, then the

difference in timescales is not a problem. Although the energy dissipation occurs over a longer timescale than the bubble creation, the net input of energy into the central regions of the cluster occurs on the bubble creation timescale. However, if the duty cycle of the central engine is short, so that bubbles are produced only rarely, then the energy dissipation timescale is the more relevant. Accurate estimates of the time-averaged energy dissipation rate are vital to the study of the energy input into the central regions of these clusters. Our study above indicated that the duty cycle is at least 70 per cent in clusters which require some form of heating. As there are a number of clusters which, although they do not have clear bubbles, have complicated central morphologies or radio emission, the duty cycle may be as high as 90 per cent.

In some clusters, Hydra A for example (Nulsen et al. 2005), there appears to have been a ‘‘cluster scale outburst.’’ In these cases the outburst may have heated the central parts of the cluster sufficiently so that it is not, currently, cooling very fast. Therefore the observed bubble size and the current cooling rate may not be as closely coupled as we have assumed. The heating effect of such large scale requires further investigation, as in these cases the ICM does not confine the bubble and the ICM pressure cannot be taken as uniform.

There exist radio sources where the morphology indicates that activity has restarted in the centre after a time of quiescence (Schoenmakers et al. 2000; Saripalli et al. 2002). Although for some of the clusters presented here even a duty cycle of 100 per cent would be insufficient to provide the energy required to off-set the X-ray cooling, for others a duty cycle of less than 100 per-cent would suffice.

For further improvements to the line of investigation we have taken, the rate of the energy dissipation into the ICM, rather than the energy injection, needs to be determined.

### 6.3 Bubble Visibility

The clusters with short cooling times are also likely to be the ones which are X-ray bright as the gas, and hence surface brightness, densities are high in the centre. Therefore the bubble-ICM contrast is also likely to be high. This could cause a selection effect for the percentage of clusters with short central cooling times in which clear bubbles have been detected. There may be bubbles in clusters without short central cooling times, but as the X-ray emission in the centre is not as bright, they have not been detected.

## 7 FURTHER WORK

During this analysis we have assumed that the energy contained within the bubble and which is available to the ICM is  $4P_{\text{th}}V$ , assuming that the bubbles are filled with a relativistic gas. Apart from energy lost to sound waves, which has been neglected in these calculations (Churazov et al. 2002),  $4P_{\text{th}}V$  is the maximum amount of energy available to offset the X-ray cooling occurring in the cluster. In some cases this energy suffices to offset the cooling out to the cooling radius, in others it falls short.

If, however, the energy were only  $P_{\text{th}}V$ , then in many more clusters the AGN would appear not to be able to offset the X-ray cooling. As a result, an important question that requires answering is whether there is  $4P_{\text{th}}V$  available in the bubble and whether it can *all* be transferred to/dissipated in the ICM?

As discussed in Section 6.2 the timescales used here to obtain the bubble powers are those for the bubble age and not those over which the bubbles would liberate their energy into the ICM. They also do not measure the time over which sound waves would dissipate. These timescales also need to be accurately measured to subsequently be able to accurately determine the heating rate of the AGN.

Recent work by Fabian et al. (2006) investigating the weak shock surrounding the bubbles in the Perseus cluster showed that the energy content of the post shock gas was around  $2P_{\text{th}}V$ . The observation that the gas across the shock is isothermal also raises the possibility that the bubbles could expand faster than the sound speed. Thermal conduction across the shock would even out any temperature differences, so making the shock less detectable. A final issue is the energy in the compressed cosmic rays and magnetic field present in the centres of clusters. Sanders *et al.* in prep show that the thermal and non-thermal pressures are comparable in the central regions of the Perseus cluster. As a result, the pressure against which the bubbles are expanding may be around double what has previously been estimated. The  $R_{\text{av}}/R_{\text{max}}$  calculation (Section 6.1) implies that this non-thermal component is important in other clusters. As these inferences come from a single cluster (albeit the X-ray brightest and best studied), further investigation is required to determine whether these properties occur in all clusters and the effect that they have on the assumptions used in AGN heating arguments.

## 8 CONCLUSIONS

We have investigated a sub-sample of the Brightest 55 cluster sample. At least 36 per cent of clusters have a cool core, and of these at least 70 per cent harbour clear bubbles. First we analysed those clusters which have a short ( $< 3 \text{ Gyr}$ ) central cooling time and a central temperature drop of a factor of two. These clusters are expected to have the most rapid cooling in the centre and so require

some form of heating. At least 36 per cent of clusters have a cool core, and of these at least 70 per cent harbour clear bubbles, implying a duty cycle also of at least 70 per cent. Up to 90 per cent could have some form of bubbles. The energy provided in the bubbles was compared to the X-ray cooling within the cooling radius (for  $r_{\text{cool}}$  at  $t_{\text{cool}} = 3 \text{ Gyr}$ ). The mean distance out to which the bubble power can offset the X-ray cooling is  $r_{\text{heat}}/r_{\text{cool}} \geq 0.86 \pm 0.11$ , with a large spread. In most clusters (10 out of 16) the AGNs energy input to the central regions of the cluster is sufficient to offset the X-ray cooling. The bubble energy in the remainder does not offset most of the X-ray cooling. In some cases this is the result of catching these bubbles at a very young age (e.g. A2199).

Also analysed were those clusters in the B55 sample which have a central radio source. The fraction of clusters which have a central radio source is at least 50 per cent. These were combined with the clusters from the previous subset which did not have clear bubbles. For clusters without clear bubbles we have used the mean value of  $r_{\text{heat}}/r_{\text{cool}}$  to estimate bubble sizes from the X-ray cooling. In five clusters (3C129.1, A2063, A2204, A3312 & A3391) the radio sources have bi-lobed morphologies, whose sizes are similar from the expected sizes. Only in two of these five clusters is the X-ray observation of sufficient depth that any interaction between the radio and ICM could be expected to be seen. It is not clear why no clear bubbles are seen, especially in A2204. As a result bubbles may be more common than previously thought.

We investigated the ratio of the actual bubble size to that of their maximum size if they were to offset all the X-ray cooling, and find the peak occurs at  $R_{\text{av}}/R_{\text{max}} \sim 0.7$  with a tail extending to higher  $R_{\text{av}}/R_{\text{max}}$ . Either we are biased to imaging young bubbles or some assumption is incorrect. A likely explanation is that a non-thermal component comparable to the thermal component is present in the innermost regions of most clusters.

## ACKNOWLEDGEMENTS

We thank Steve Allen, Roderick Johnstone, Jeremy Sanders and James Graham for interesting discussions during the course of this work. ACF and RJHD acknowledge support from The Royal Society and PPARC respectively. All plots in this manuscript were created with *Veusz*.

## REFERENCES

- Allen S. W., Dunn R. J. H., Fabian A. C., Taylor G. B., Reynolds C. S., 2006, MNRAS, in press astro-ph/0602549
- Arnaud K. A., 1996, in Jacoby G. H., Barnes J., ed, ASP Conf. Ser. 101: Astronomical Data Analysis Software and Systems V, p. 17
- Birzan L., Rafferty D. A., McNamara B. R., Wise M. W., Nulsen P. E. J., 2004, ApJ, 607, 800
- Blanton E. L., Sarazin C. L., McNamara B. R., Wise M. W., 2001, ApJ, 558, L15
- Böhringer H., Voges W., Fabian A. C., Edge A. C., Neumann D. M., 1993, MNRAS, 264, L25
- Burns J. O., 1990, AJ, 99, 14
- Churazov E., Brüggen M., Kaiser C. R., Böhringer H., Forman W., 2001, ApJ, 554, 261
- Churazov E., Forman W., Jones C., Böhringer H., 2000, A&A, 356, 788

- Churazov E., Sunyaev R., Forman W., Böhringer H., 2002, *MNRAS*, 332, 729
- Donahue M., Horner D. J., Cavagnolo K. W., Voit G. M., 2006, *ApJ*, 643, 730
- Donahue M., Voit G. M., O’Dea C. P., Baum S. A., Sparks W. B., 2005, *ApJ*, 630, L13
- Dunn R. J. H., Fabian A. C., 2004, *MNRAS*, 351, 862
- Dunn R. J. H., Fabian A. C., Sanders J. S., 2006, *MNRAS*, 366, 758
- Dunn R. J. H., Fabian A. C., Taylor G. B., 2005, *MNRAS*, 364, 1343
- Edge A. C., Stewart G. C., Fabian A. C., Arnaud K. A., 1990, *MNRAS*, 245, 559
- Fabian A. C., Reynolds C. S., Taylor G. B., Dunn R. J. H., 2005, *MNRAS*, 363, 891
- Fabian A. C., Sanders J. S., Allen S. W., Crawford C. S., Iwasawa K., Johnstone R. M., Schmidt R. W., Taylor G. B., 2003a, *MNRAS*, 344, L43
- Fabian A. C., Sanders J. S., Crawford C. S., Conselice C. J., Gallagher J. S., Wyse R. F. G., 2003b, *MNRAS*, 344, L48
- Fabian A. C., Sanders J. S., Taylor G. B., Allen S. W., Crawford C. S., Johnstone R. M., Iwasawa K., 2006, *MNRAS*, 366, 417
- Furusho T., Yamasaki N. Y., Ohashi T., 2004, *Advances in Space Research*, 34, 2530
- Ghizzardi S., Molendi S., Pizzolato F., De Grandi S., 2004, *ApJ*, 609, 638
- Johnstone R. M., Allen S. W., Fabian A. C., Sanders J. S., 2002, *MNRAS*, 336, 299
- Johnstone R. M., Fabian A. C., Morris R. G., Taylor G. B., 2005, *MNRAS*, 356, 237
- Kim W.-T., Narayan R., 2003, *ApJ*, 596, 889
- Marković T., Owen F. N., Eilek J. A., 2004, in Reiprich T., Kempner J., Soker N., ed, *The Riddle of Cooling Flows in Galaxies and Clusters of galaxies*, p. 61
- Mazzotta P., Edge A. C., Markevitch M., 2003, *ApJ*, 596, 190
- Mazzotta P., Kaastra J. S., Paerels F. B., Ferrigno C., Colafrancesco S., Mewe R., Forman W. R., 2002, *ApJ*, 567, L37
- McNamara B. R. et al., 2000, *ApJ*, 534, L135
- Mewe R., Kaastra J. S., Leidahl D. A., 1995, *Legacy*, 6, 16
- Morganti R., Oosterloo T., Tadhunter C. N., Aiudi R., Jones P., Villar-Martin M., 1999, *A&AS*, 140, 355
- Nulsen P. E. J., McNamara B. R., Wise M. W., David L. P., 2005, *ApJ*, 628, 629
- Otani C., Brinkmann W., Böhringer H., Reid A., Siebert J., 1998, *A&A*, 339, 693
- Peres C. B., Fabian A. C., Edge A. C., Allen S. W., Johnstone R. M., White D. A., 1998, *MNRAS*, 298, 416
- Peterson J. R., Fabian A. C., 2006, *Physics Reports*, 427, 1
- Peterson J. R., Kahn S. M., Paerels F. B. S., Kaastra J. S., Tamura T., Bleeker J. A. M., Ferrigno C., Jernigan J. G., 2003, *ApJ*, 590, 207
- Pratt G. W., Arnaud M., Pointecouteau E., 2006, *A&A*, 446, 429
- Rafferty D. A., McNamara B. R., Nulsen P. E. J., Wise M. W., 2006, *astro-ph/0605323*
- Sanders J. S., Fabian A. C., 2002, *MNRAS*, 331, 273
- Sanders J. S., Fabian A. C., Dunn R. J. H., 2005, *MNRAS*, 360, 133
- Sanders J. S., Fabian A. C., Taylor G. B., 2005, *MNRAS*, 356, 1022
- Saripalli L., Subrahmanyam R., Udaya Shankar N., 2002, *ApJ*, 565, 256
- Schoenmakers A. P., de Bruyn A. G., Röttgering H. J. A., van der Laan H., Kaiser C. R., 2000, *MNRAS*, 315, 371
- Takizawa M., Sarazin C. L., Blanton E. L., Taylor G. B., 2003, *ApJ*, 595, 142
- Taylor G. B., Govoni F., Allen S. W., Fabian A. C., 2001, *MNRAS*, 326, 2
- Voigt L. M., Fabian A. C., 2004, *MNRAS*, 347, 1130
- Voigt L. M., Fabian A. C., 2006, *MNRAS*, 368, 518

## APPENDIX

Here we present the temperature, density, pressure, entropy, cooling time and cumulative heating profiles for the clusters in our sample which harbour clear bubbles.

As can be seen from the figures, the temperature profiles (Fig. 9) do not lie on top of each other, but the central temperature drops can be seen in these clusters. The electron density profiles are much more uniform and much smoother. These features carry into the derived profiles; the pressure’s do not lie on top of each other and fall as expected with radius.

The entropy<sup>7</sup> and cooling time profiles for the clusters are very similar. The scatter about the general trends are much less in these profiles than in the others. The overall shape of these profiles are similar to those in Pratt et al. (2006); Voigt & Fabian (2004).

We have fitted simple powerlaws to all of the profiles of the clusters individually. The mean, maximum and minimum are given in the figure captions. In some cases the values for the outermost shell have been ignored when this is obviously different from a global trend (Johnstone et al. 2005). If a shell has not been used for a fit in the density or temperature, it has not been used any of the fits in subsequent derived profiles.

<sup>7</sup> We use  $S = kTn_e^{-2/3}$  as a proxy for the true entropy.

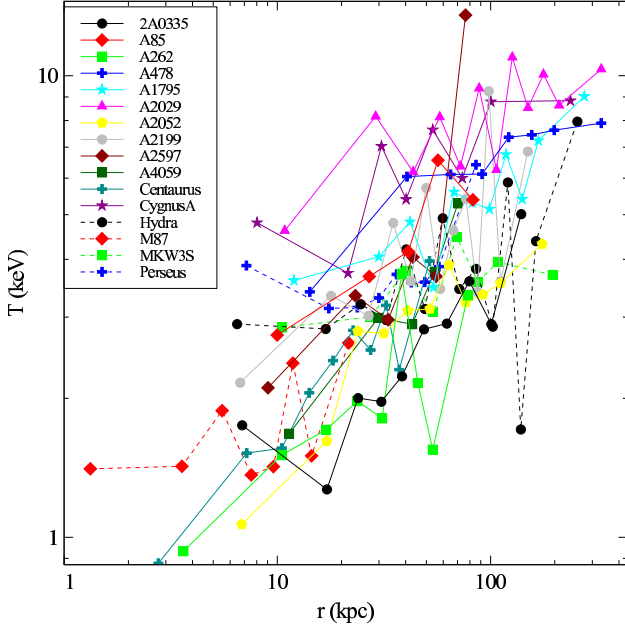


**Figure 9.** The temperature profiles of all the clusters in the sample which harbour clear bubbles. Error bars have been omitted for clarity. The  $1 - \sigma$  errorbars are  $\sim 2 - 10$  per cent at 10 kpc and  $\sim 0.6 - 15$  per cent at 100 kpc. The average powerlaw index is 0.32 with a range of 0.11 – 0.59.

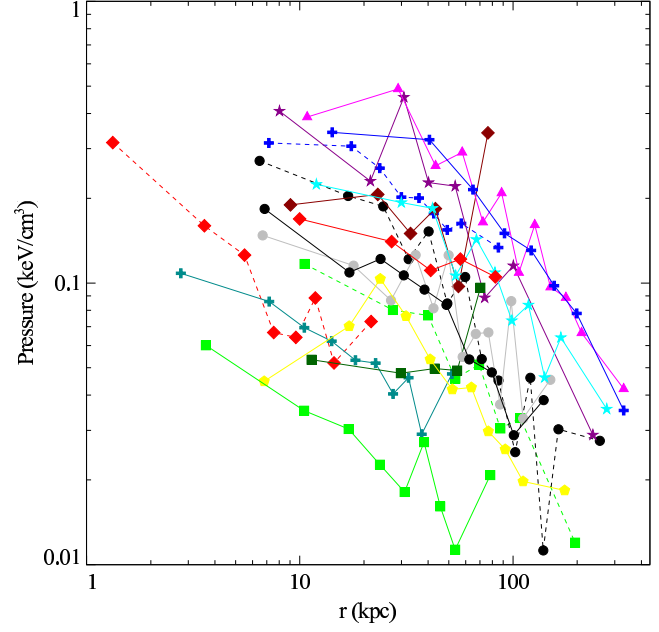


**Figure 11.** The pressure profiles of all the clusters in the sample which harbour clear bubbles. The legend is missing deliberately, but is the same as the other profiles. The average powerlaw index is  $-0.60$  with a range of  $-0.09$  to  $-1.13$ .

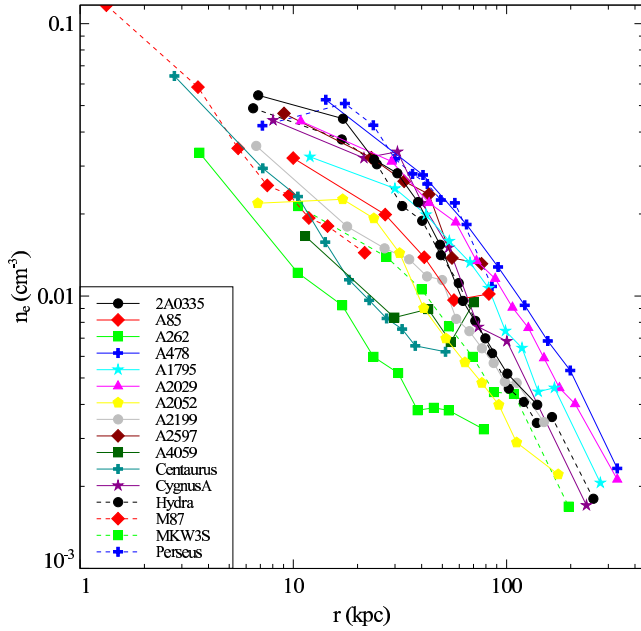


**Figure 10.** The electron density profiles of all the clusters in the sample which harbour clear bubbles. Error bars have been omitted for clarity. The  $1 - \sigma$  errorbars are  $\sim 1 - 3$  per cent at 10 kpc and  $\sim 2$  per cent at 100 kpc. The average powerlaw index is  $-0.90$  with a range of  $-0.13$  to  $-1.34$ .

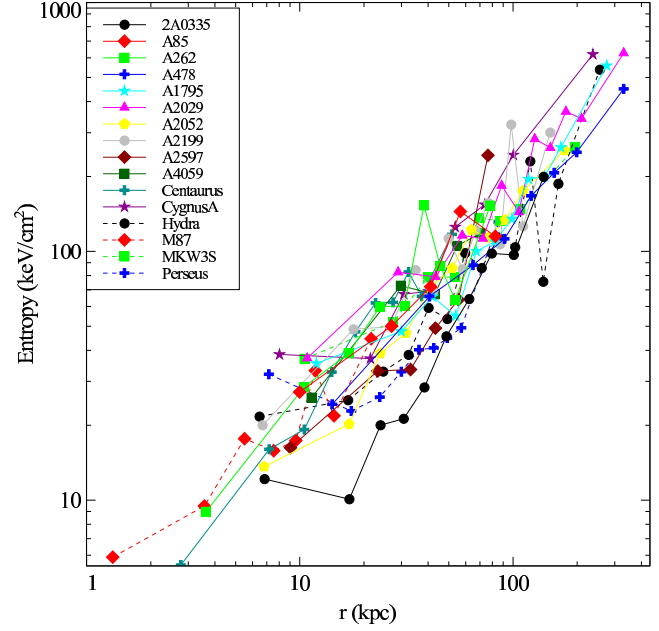


**Figure 12.** The entropy profiles of all the clusters in the sample which harbour clear bubbles. The average powerlaw index is 0.94 with a range of 0.68 – 1.41.

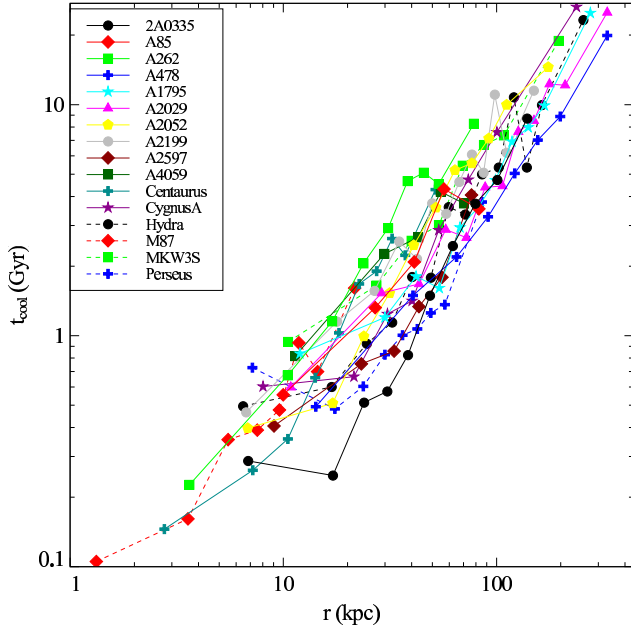


**Figure 13.** The cooling time profiles of all the clusters in the sample which harbour clear bubbles. The average powerlaw index is 1.19 with a range of 0.83 – 1.76.

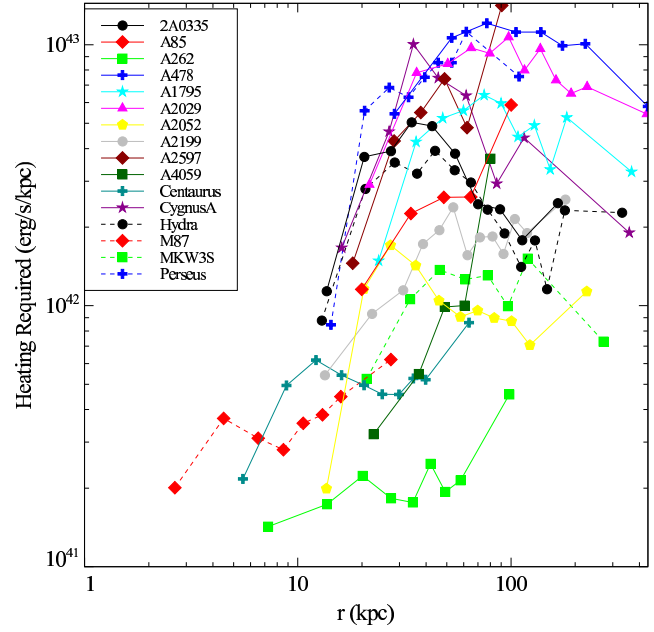


**Figure 15.** The profiles of all the clusters in the sample which harbour clear bubbles showing the amount of power required to offset the X-ray cooling per kpc.

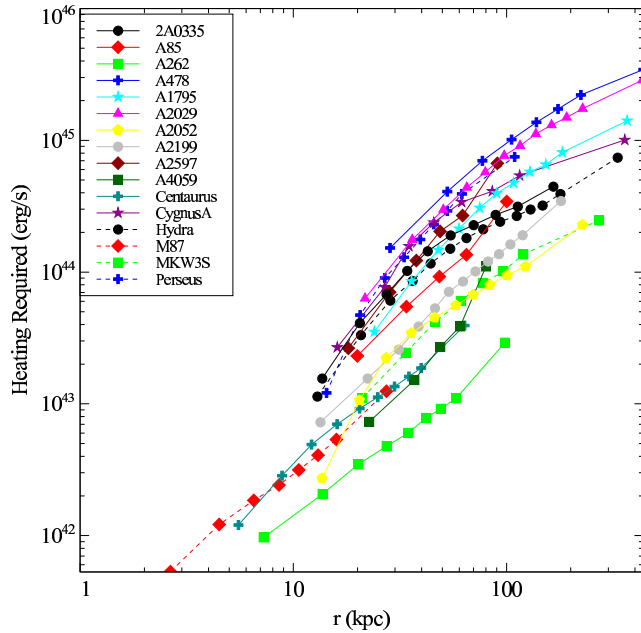


**Figure 14.** The profiles of all the clusters in the sample which harbour clear bubbles showing the cumulative amount of power required to offset the X-ray cooling. Note that the differential of these curves, the heating ratio per kpc, is approximately flat (Fig. 15). The average powerlaw index is 1.40 with a range of 0.80 – 2.09.